Age-related reorganization of functional network architecture for language processing

Running title: Age-related reorganization of functional networks in language

Sandra Martin[1,2*], Kathleen A. Williams[1], Dorothee Saur[2], Gesa Hartwigsen[1]

[1] Lise Meitner Research Group Cognition and Plasticity, Max Planck Institute for Human Cognitive and Brain Sciences, Leipzig, Germany

[2] Language & Aphasia Laboratory, Department of Neurology, University of Leipzig Medical Center, Leipzig, Germany

Main text word count: 4996

Abstract: 150

Number of Figures: 6

Number of Tables: 2

*Correspondence should be addressed to:
Sandra Martin
Lise Meitner Research Group Cognition & Plasticity
Max Planck Institute for Human Cognitive and Brain Sciences
Stephanstr. 1a
04103 Leipzig, Germany
martin@cbs.mpg.de
phone: +49 341 99402683

Abstract

Cognitive aging is associated with widespread neural reorganization processes in the human brain. However, the behavioral impact of such reorganization is not well understood. The current neuroimaging study investigated age differences in the functional network architecture during language production. Combining task-based functional connectivity, graph theory and cognitive measures of fluid and crystallized intelligence, our findings show age-accompanied large-scale network reorganization even when older adults have intact word retrieval abilities. In particular, functional networks of older adults were characterized by reduced decoupling between systems, reduced segregation and efficiency, and a larger number of hub regions relative to young adults. Exploring the predictive utility of these age-related changes in network topology revealed high, albeit less efficient, performance for older adults whose brain graphs showed stronger dedifferentiation and reduced distinctiveness. Our results have important implications for theoretical accounts of neurocognitive aging, indicating a successful compensatory network reconfiguration at the cost of efficient wiring.

Keywords: aging, functional connectivity, semantic memory, graph theory, language production

Introduction

Communication is an essential human ability for everyday life. It draws on the general knowledge of words, concepts, and ideas we accumulate across the lifespan, so-called semantic memory, as well as personal experiences, also referred to as episodic memory[1]. Although communication abilities remain largely intact in healthy aging, and copious evidence has shown preservation or even increases in semantic memory through adulthood into very old age[2–4], memory problems in verbal communication, such as finding the right word and tip-of-the-tongue episodes, are a common complaint with increasing age[5]. This paradox has been explained in terms of less efficient access and retrieval processes during language production that rely on semantic and cognitive control functions like working memory, attention, and inhibitory control, and are well established to steadily decline with age[6]. Thus, the impact of aging on communicative abilities may vary as a function of an individual's cognitive control abilities and intact semantic memory. However, little is known about the neural mechanisms underlying those subtle changes in communicative abilities with age.

The recent conceptualization of the brain as a complex modular system[7,8] provides a unique framework to examine age-related changes in neural information processing and their consequences for behavior. To this end, graph-theoretical measures offer an analytical method to model such complex systems and explore organization principles of human brain networks[9,10]. Links between functional connectivity within and across specialized modules or neural networks and cognitive outcomes in young adults have revealed a topological organization of the brain that combines local information processing with global information integration aimed at optimizing global cost efficiency ("small world" organization)[11,12]. Age-related changes to this modular organization have been described as a general decline of functional network segregation evident in the form of decreased within- and enhanced between-network functional connectivity[13–15]. Moreover, increasing age has been associated with reduced small-world organization, modularity, and local and global efficiency of functional brain networks[16–19]. The impact of such reorganization on cognition remains debated. Most studies associated neural dedifferentiation with performance decline[13,18,20], whereas some have pointed towards a pattern of compensational response, where reduced network segregation counteracts the age-related decline of brain function to maintain successful performance[15].

While the majority of studies investigated functional connectivity from resting-state functional magnetic resonance imaging (fMRI), important insight can be gained through task-based functional connectivity. Interestingly, age-accompanied differences in network topology during task processing largely concur with reported patterns in resting-state in the form of stronger integration and reduced segregation[21–23]. However, their behavioral relevance seems to depend on the cognitive resources required for the task of interest. Research from domains well known to steadily decline with age, such as episodic and working memory, reported compensational recruitment of control and attention networks for successful performance[21,24,25] but also maintenance processes with age to preserve

neural resources despite structural deterioration[26,27]. A different picture emerges for cognitive abilities that remain stable with age like language and creativity. Here, increased connectivity between usually anti-correlated networks such as executive and default networks might be advantageous for older adults when access to semantic memory and little cognitive control are required so that they can rely on prior knowledge to maintain high performance[23,28,29].

Despite its relevance for successful verbal communication, research on age-related network organization during semantic word retrieval is sparse. In this context, semantic fluency tasks are especially valuable since they tap into semantic memory but also cognitive control processes and are often linked to preserved albeit slower performance in older adults[30]. Previous studies revealed age-related reduced functional connectivity within domain-specific networks during semantic word retrieval, however, without affecting behavioral performance[31,32]. Furthermore, we recently showed that functional connectivity within and between domain-general networks like the default and multiple-demand network differently impacts the behavior of older and young adults during a semantic fluency task, even when network coupling is age-invariant[29]. Thus, domains that are usually well-preserved with age offer an opportunity to inform the current understanding of age-accompanied changes in the architecture of functional brain networks and their behavioral relevance regarding compensatory and aberrant mechanisms.

The present study addresses this gap by exploring age-related reorganization of functional networks during processing of a semantic word retrieval task. Networks of task-based functional connectivity in groups of healthy young and older adults were derived via data-driven, multivariate methods. We were interested in age differences in the coupling of task-relevant networks and their behavioral relevance. Furthermore, we applied graph-theoretical measures of brain system segregation, integration, and network hubs to investigate the network topology in young and older adults. Leveraging recent advances in network neuroscience, we used orthogonal minimum spanning trees[33] (OMST) for the calculation of graph measures to avoid arbitrary thresholding of functional connectivity matrices[34]. These measures were then related to participants' in-scanner task performance and abilities of fluid and crystallized intelligence to examine the prognostic utility of age-related changes in brain network topology. Exploring task-based network topologies as a function of cognitive performance in a domain that is usually well preserved with age enabled us to gain key insights into age-related reorganization processes within subjects and to inform theoretical accounts regarding compensatory and detrimental effects of neurocognitive aging on behavior.

Results

The main objective of this study was to investigate age-related changes in integration and segregation of functional neural networks engaged in the goal-directed access to semantic memory. By contrasting a paced overt semantic fluency task with an overt counting task, we delineated neural networks specific to semantic access and control processes in healthy young (n = 30, mean = 27.6 years, SD = 4.3, range = 21–34) and older adults (n = 31, mean = 65.5 years, SD = 2.75, range = 60–69 years). Due to strong in-scanner motion (>1 voxel size), data from three older participants had to be excluded from further analyses, leading to a final sample size of 28 participants in the older group. While both groups were matched for gender, participants in the young group had significantly more years of education ($t(55.86) = 5.21$, $p < 0.001$). During one experimental session, participants completed two runs of the fMRI experiment (Figure 1a) followed by a neuropsychological assessment probing semantic knowledge as well as verbal- and non-verbal executive functions (Table 1). Consistent with previous research, older adults only performed better for the measure of semantic memory (spot-the-word test; $t(54.39) = 3.14$, $p = 0.003$), indicating a maintenance of semantic knowledge and an increase in vocabulary with age[4], while young adults performed better on all other tests (all at $p < 0.01$), which is consistent with the assumption of a general age-related decline of executive functions[6]. For all reported correlation analyses, neuropsychological measures were summarized via exploratory factor analysis (Methods). Results revealed an “executive functions” factor with high loadings on Trail Making Tests A (0.8) and B (0.71), Digit Symbol Substitution Test (0.73), and reading span test (0.45), and a “semantic memory” factor with spot-the-word test (0.5) and verbal fluency tests for hobbies (0.44) and surnames (0.98). For the in-scanner tasks, we fitted mixed-effects models accounting for individual variance of participants and semantic categories via random effects and the difference in years of education via covariate (Table S1). Likelihood-ratio tests showed that both age groups performed similarly ($x^2 = 2.18$, $p = 0.14$) and generally better for counting than semantic fluency ($x^2 = 8.06$, $p = 0.005$; Figure 1b). For response time, results showed an interaction between task and age group ($x^2 = 79.73$, $p < 0.001$) with older adults performing slower than young adults during the semantic fluency but not the counting task (Figure 1c).

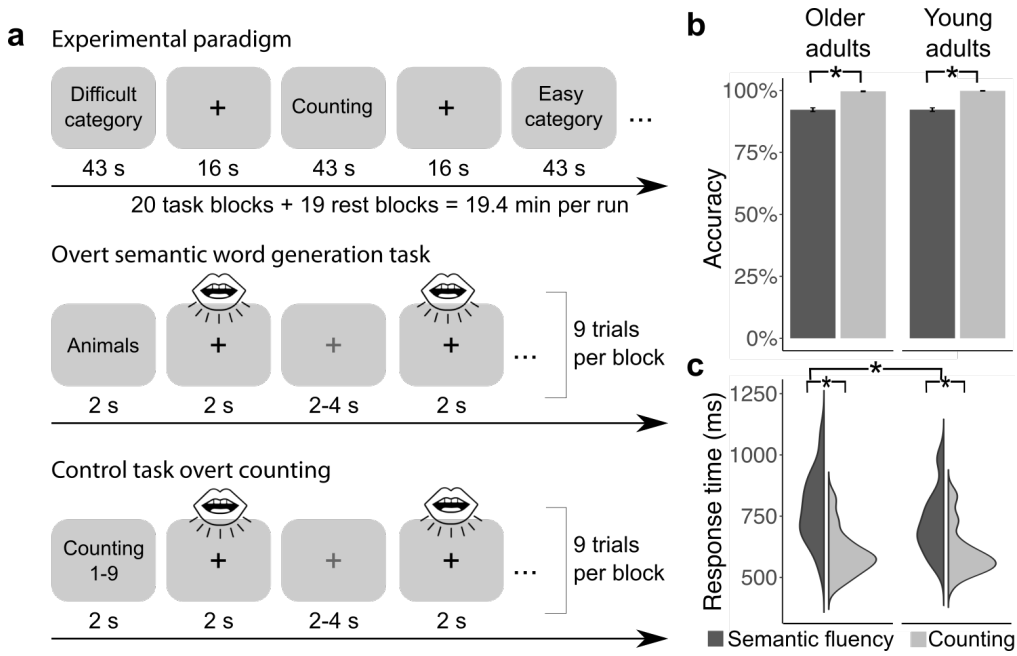

Figure 1. Experimental design. (a) The fMRI experiment consisted of 43-s task blocks of overt paced semantic fluency and counting, which were presented in a pseudorandomized order and separated by 16-s rest periods. Two examples for each task are shown. There were 10 blocks per run for each task. At the beginning of a task block, a 2 s visual word cue indicated whether participants were expected to generate category exemplars or count forward (1 to 9) or backward (9 to 1). Participants were instructed to produce exactly one exemplar for a category or to say one number when the fixation cross turned green and to pause when the cross turned red. If they could not think of an exemplar, they were instructed to say “next”. Each task block contained 9 trials of the same semantic category/counting task which were separated by jittered inter-stimulus intervals. (b) and (c) show behavioral results for each task and age group. While results revealed better performance for counting than semantic fluency in both groups but no difference in accuracy between age groups, older adults performed slower during semantic fluency than young adults.

Table 1. Characteristics and neuropsychological test results of participants

	Young adults (*n* = 30)	Older adults (*n* = 28)
Demographics		
Age (years)	27.6 (4.4)	65.2 (2.8)
Gender (F:M)	16:14	14:14
Education (years)	18.7 (2.6)	15.2 (2.5)*
Beck Depression Inventory (cut-off 18 points)	–	4.7 (4.1)
Neuropsychological		
Spot-the-word test (max. 40)	29.1 (3.2)	31.5 (2.5)*
Semantic fluency (sum surnames, hobbies)	51.2 (8.4)	40.7 (6.7)*
Reading span test (max. 6)	3.5 (1)	2.9 (0.7)*
Digit symbol substitution test (max. 90 in 90 s)	72.1 (11.4)	50.2 (10.4)*
Trail Making Test A (time in s)	17.3 (5.8)	25.4 (6.4)*

Trail Making Test B (time in s)	36.1 (11.9)	61.8 (29.4)*
Mini-Mental State Examination (max. 30 points)	–	28.36 (1.2)

Note. Mean values of raw scores with standard deviations. * Significant differences between age groups at $p < 0.01$.

Goal-directed access to semantic memory involves default, semantic, and executive control networks

Using the data-driven method of group spatial independent component analysis (ICA) on the whole data set, we defined functional cortical networks for the semantic task. The ICA identified 55 components of which 42 were clearly attributable to artifacts. From the resulting 13 non-noise components, low-level sensory components including auditory, sensorimotor, and visual networks were identified and removed since their roles were beyond the scope of our investigation. For reference, all independent components are displayed in Figure S1.

The remaining seven components were submitted to one-sample t-tests and thresholded controlling the family-wise error (FWE) rate at peak level with $p < 0.05$ and a cluster-extent threshold of 10 voxels. Figure 2 shows the thresholded maps with their original component number. To determine which cognitive network best described each component, we calculated the Jaccard similarity coefficient (J) between our thresholded, binarized components of interest and template masks of common resting-state[35] and semantic cognition networks[36]. Results showed similarity above threshold ($J = 0.15$) for all component maps with distinct cognitive networks (Table 2). For IC06, we found overlap with the frontoparietal control network C (CONT-C) and default mode network A (DMN-A). Although spatial similarity was marginally higher for CONT-C than DMN-A ($J_{\text{Control C}} - J_{\text{Default A}} = 0.01$), we refer to this component as part of the default system. Significant clusters included classic midline structures of the core default network[37] like posterior cingulate cortex, precuneus, and prefrontal cortex (Figure 2). An additional analysis of similarity coefficients between the component maps and the 7-networks parcellation[35] revealed a stronger similarity with the default network as a whole for this component ($J_{\text{Control}} - J_{\text{Default}} = -0.03$; see Table S2 for results with the 7-networks parcellation). Furthermore, a second component (IC13) showed strong similarity with DMN-A. As described in Methods, we combined the component maps of IC06 and IC13 to assess whether this would lead to a numerical improvement of J. Results showed that this was not the case with $J = 0.21$ for the combined components which was below the similarity coefficient of IC13 alone ($J = 0.26$). Thus, both components represented distinct parts of DMN-A and were hence included in subsequent analyses. For IC13, we further included default mode network C (DMN-C), which showed the second strongest overlap and was represented by significant clusters in bilateral parahippocampal gyri. Indeed, a combined template of DMN-A and DMN-C led to a numerical improvement in similarity compared to DMN-A alone ($J_{\text{Default A + C}} - J_{\text{Default A}} = 0.091$). Thus, to gain

197 a comprehensive representation of the default network, both subsystems were combined and are
198 referred to as default mode network A+C (DMN-A+C).
199 Results of Jaccard calculations further revealed the following networks for the other
200 components: default mode network B (DMN-B; IC16) with peak activations in bilateral middle
201 temporal gyri (MTG), inferior and superior frontal gyri (IFG, SFG), and left angular gyrus (AG);
202 semantic network (SEM; IC18) with strong overlap with the semantic control network and peak
203 activations in left IFG, SFG, paracingulate gyrus, posterior superior temporal gyrus (STG), and AG;
204 frontoparietal control network B (CONT-B; IC09) with large clusters in bilateral SFG and middle
205 frontal gyri (MFG), AG, and posterior MTG; ventral attention network B (VAN-B; IC45) with peak
206 activation in prefrontal cortex including paracingulate gyrus, bilateral IFG and supramarginal gyri;
207 and dorsal attention network A (DAN-A; IC52) with large clusters in bilateral AG, and
208 temporooccipital cortex. Statistical tables with all significant clusters are reported in Supplementary
209 Table S3. The overlap between each component and the selected cognitive network is shown in
210 Figure 2.

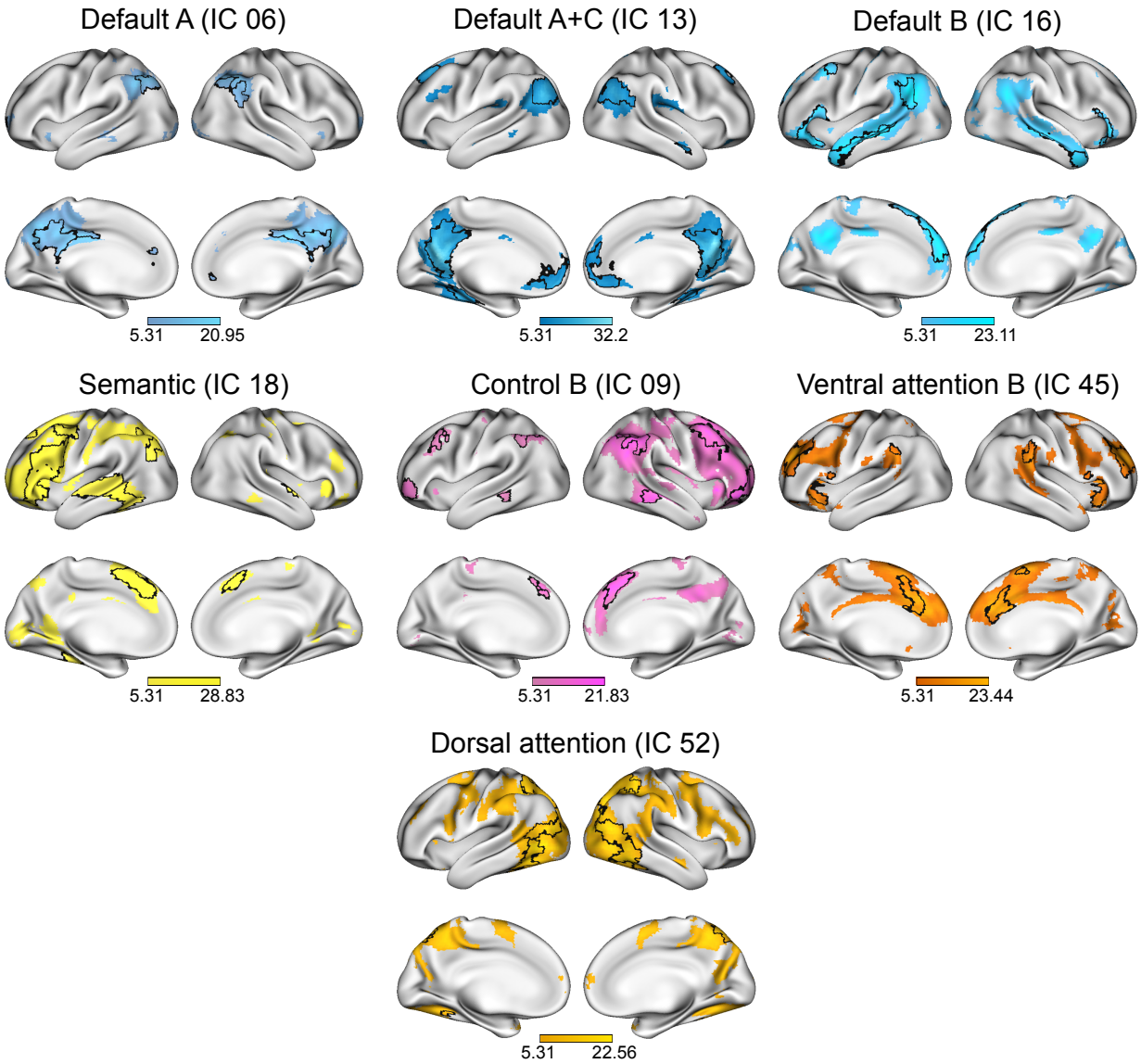

Figure 2. ICA-derived networks and their overlap with cognitive networks. T-scores from one-sided t-tests (FWE-corrected $p < 0.05$ at peak level) are displayed for the seven selected component maps with their respective network label according to spatial similarity analysis. Overlaps between the thresholded component map and the spatially most similar cognitive network according to the Jaccard index are outlined on the surface of the brain. The areas of overlap were used for subsequent network analyses.

Table 2. Jaccard indices for independent components and cognitive networks

	IC06	**IC09**	**IC13**	**IC16**	**IC18**	**IC45**	**IC52**
Frontoparietal control A	0.054	0.133	0.032	0.013	*0.151*	0.083	0.109
Frontoparietal control B	0.091	**0.210**	0.028	0.073	0.125	0.050	0.018
Frontoparietal control C	*0.168*	0.020	0.066	0.010	0.010	0.028	0.044
Default A	**0.154**	0.089	**0.255**	0.149	0.040	0.054	0.019
Default B	0.039	0.069	0.031	**0.263**	0.082	0.098	0.010

Default C	0.014	0.010	**0.122**	0.008	0.026	0.001	0.020
Dorsal attention A	0.051	0.041	0.062	0.015	0.054	0.003	**0.180**
Dorsal attention B	0.008	0.038	0.006	0.006	0.071	0.053	0.123
Limbic A	0.000	0.001	0.002	0.014	0.002	0.002	0.011
Limbic B	0.001	0.007	0.015	0.004	0.009	0.005	0.002
Ventral attention A	0.042	0.012	0.023	0.015	0.033	0.124	0.065
Ventral attention B	0.014	0.074	0.001	0.031	0.059	**0.195**	0.039
Somatomotor A	0.022	0.052	0.000	0.039	0.036	0.029	0.028
Somatomotor B	0.000	0.016	0.038	0.009	0.033	0.011	0.015
Temporal parietal	0.001	0.029	0.014	0.118	0.023	0.035	0.034
Central visual	0.022	0.006	0.006	0.038	0.011	0.004	0.123
Peripheral visual	0.025	0.009	0.074	0.020	0.038	0.034	0.037
General semantic cognition	0.032	0.030	0.072	*0.194*	**0.201**	0.092	0.050
Semantic control	0.012	0.036	0.012	0.067	*0.153*	0.091	0.027

Note. The selected network labels for the respective independent components are shown in bold while all cognitive networks that showed a higher similarity coefficient than $J = 0.15$ are shown in italics.

Stronger coupling of default and executive systems predicts intact but less efficient semantic retrieval in older adults

Following rigorous quality control and data-cleaning procedures (Methods), functional brain networks (graphs) were constructed based on the seven networks derived from the ICA. For each participant, a graph consisting of seven nodes each representing one network, as well as a graph with 121 nodes based on significant clusters within each network (see Figure 4a for all 121 nodes) were created. Graphs were then submitted to correlational psychophysiological interaction analyses (cPPI)[38] to extract task-related connectivity for our condition of interest (semantic fluency). In contrast to traditional PPI analysis, cPPI results in undirected, symmetric matrices that can be submitted to network analyses. We tested for statistically significant coupling differences between age groups by means of network-based statistics using permutation testing while controlling for in-scanner head motion (Figure 3a). Overall, the network of older adults showed reduced decoupling compared to young adults. This was especially the case for connectivity across different networks as shown by subsystems of the default network that were less decoupled from attention networks. Significantly stronger positive coupling was found in the graphs of older adults for the networks SEM with VAN-B, CONT-B with VAN-B, and DAN-A with VAN-B. A similar picture of age-related differences emerged for the more fine-grained graphs containing 121 nodes. Here, young adults

generally showed stronger positive coupling within individual networks and between subsystems of the default network and stronger decoupling between different networks (Figure S2).

We probed the behavioral relevance of the network connection pairs that showed significant age differences by calculating mixed-effects models for accuracy and response time data (Figure 3b; Table S4-5). These models and all subsequent reported models controlled for years of education and head motion defined as average framewise displacement (FD) and included random intercepts for participants and semantic categories. Continuous predictors were always mean-centered before model estimation. Reported significant effects are based on likelihood-ratio tests. Results were corrected for multiple comparisons using the Bonferroni-Holm method. For accuracy, we found significant interactions between age and between-network connectivity for VAN-B with DMN-A+C (x^2= 12.39, p = 0.002) and DAN-A (x^2= 14.18, p < 0.001). Predicting response time revealed significant interactions between age and between-network connectivity for VAN-B with DMN-A+C (x^2= 5.65, p = 0.035), SEM (x^2= 25.75, p < 0.001), and DAN-A (x^2= 28.81, p < 0.001), and for DAN-A with DMN-B (x^2= 51.76, p < 0.001). For older adults, increased coupling between default and attention networks predicted high but less efficient performance, while increased coupling of SEM and VAN-B and between both attention systems (DAN-A and VAN-B) was associated with faster responses. A different picture emerged in young adults, where stronger coupling between default and executive systems predicted faster but poorer performance while increased connectivity between DAN-A and VAN-B was associated with better and faster reactions. These results suggest that both age groups showed distinct connectivity profiles, with older adults generally profiting from increased coupling between different cognitive systems and the opposite pattern for young adults.

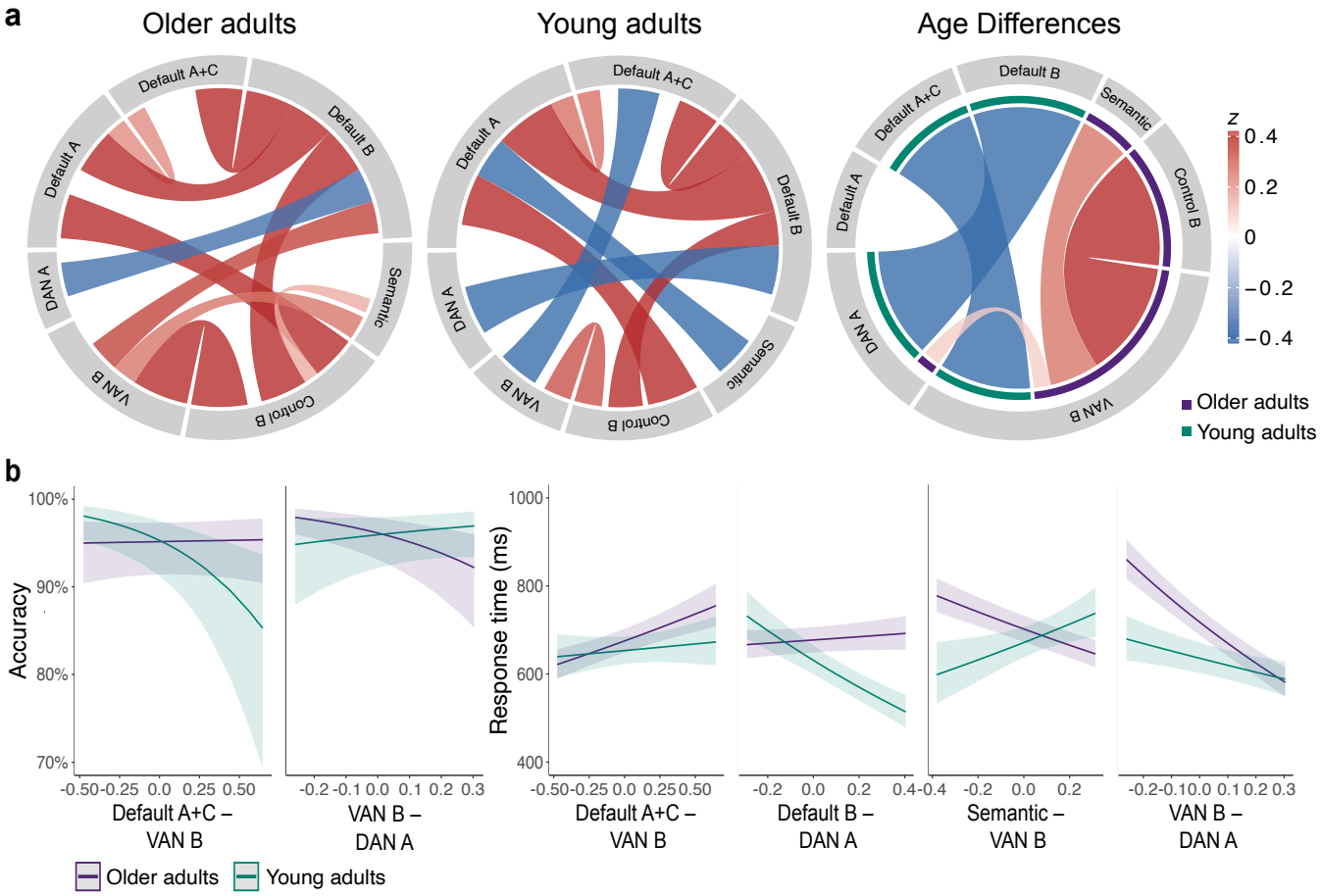

Figure 3. Functional coupling between task-relevant networks in young and older adults and their behavioral relevance. (a) Chord diagrams display significant results of functional coupling between the ICA-derived networks. Connectivity values are partial correlations. The color intensity and width of a connection indicate its correlational strength. Red indicates coupling and blue indicates decoupling between networks. Chord diagrams of each age group are based on cPPI-derived significance values while age differences were assessed using permutation testing in network-based statistics (cluster-forming threshold at p = 0.01, FWE-corrected significance threshold at p = 0.05 with 10,000 permutations). (b) Network connections that showed significant age differences were probed for their behavioral relevance. Plots show significant two-way interactions between age and the respective network pair for accuracy and response time data. Connectivity values were mean-centered for interaction analyses. Results were corrected for multiple comparisons using the Bonferroni-Holm method at p = 0.05. VAN ventral attention network, DAN dorsal attention network.

Reduced segregation and higher integration of task-relevant networks is associated with better and more efficient performance in older adults

Next, we investigated brain system segregation and integration to get a better understanding of age-related differences in whole-brain dynamics (Figure 4a). Segregation quantifies the presence of densely connected regions that form distinct subnetworks or communities in a global brain network (Figure 4b). In functional connectivity networks, such communities are indicative of functional specialization and segregated neural processing[9,10]. Results of a linear mixed-effects model for global brain system segregation revealed a significant effect of age (x^2= 11.23, p < 0.001) with

young adults exhibiting stronger segregation than older adults (Figure 4c; Table S6). Examining the predictive value of segregation for in-scanner performance and neuropsychological measures revealed significant interactions between age and segregation for accuracy (x^2= 9.54, p = 0.002), response time (x^2= 71.15, p < 0.001), and a significant correlation of segregation with executive functions in young adults (r = 0.45, p = 0.013). For all interactions, increasing levels of segregation predicted better and faster performance in young adults. In contrast, increasing brain-wide segregation had no effect on accuracy but predicted faster responses in older adults (Figure 4c; Table S7).

We used the measure of global efficiency to assess network integration. Global efficiency is calculated as the inverse of the sum of shortest paths between all nodes in a network and is thus a measure of efficient signal transmission[39]. In brain networks, it is used to assess their capacity for parallel information transfer and integrated processing[11]. Like most graph theoretical measures, the calculation of global efficiency requires a sparse graph to represent a biologically plausible network of functional connectivity[40]. Following recent work on the most reliable and representative construction of brain networks[33,40,41], we calculated individual OMST based on the weighted functional connectivity matrices and used the OMST to assess global efficiency. A linear mixed-effects model indicated higher global efficiency for young adults (x^2= 21.86, p < 0.001; Figure 4d; Table S8). Efficiency values were then entered into regression models to assess their predictive value. Results showed a significant main effect of global efficiency for accuracy (x^2= 8.79, p = 0.003) and a significant interaction with age for response time (x^2= 41.79, p < 0.001). While increasing system-wide efficiency was generally associated with better performance, it also predicted faster performance in older adults but slower responses in young adults (Figure 4d; Table S9).

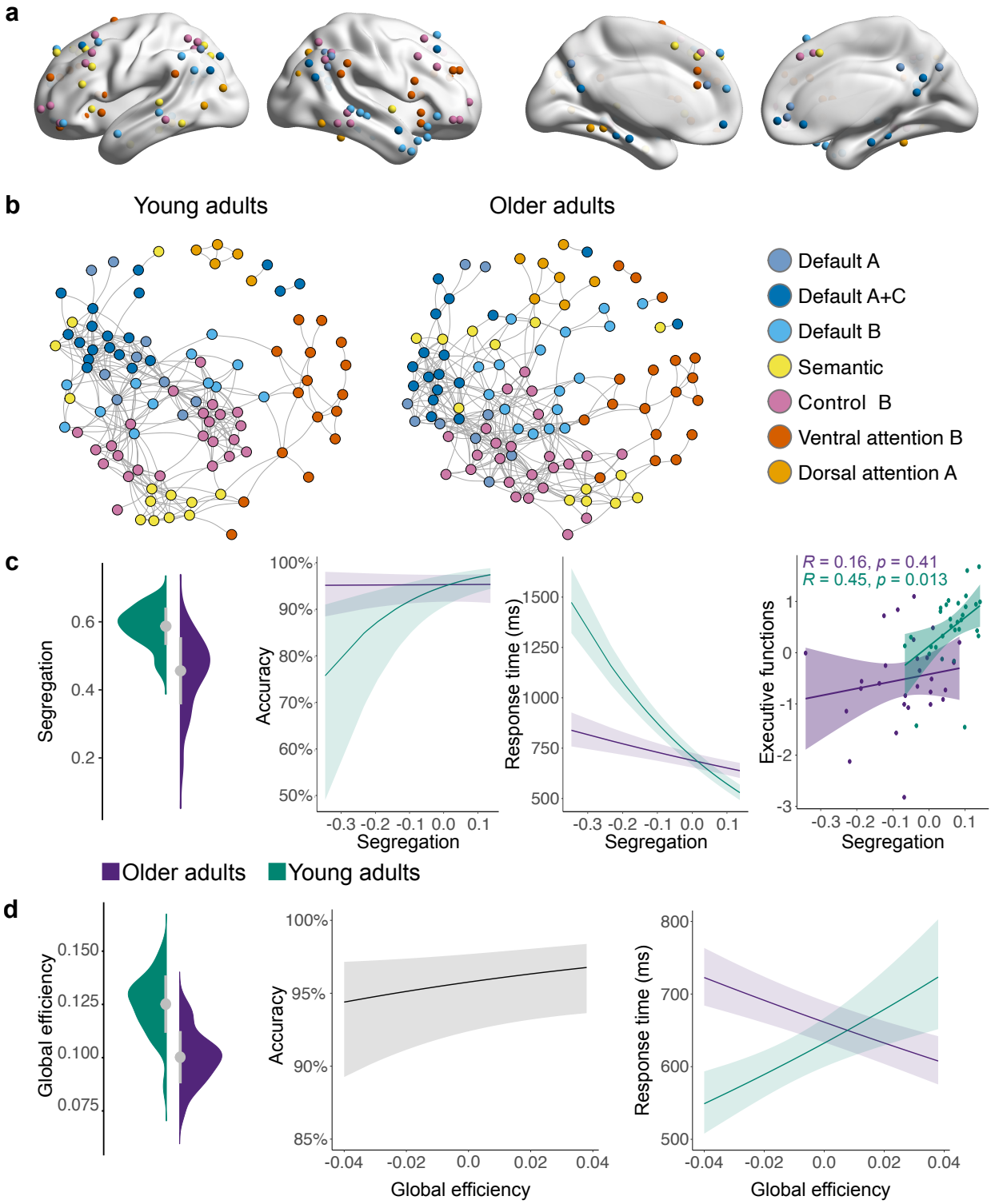

Figure 4. Age-related differences in whole-brain segregation and integration and their behavioral relevance. (a) For each participant, a task-related brain network graph was constructed using 121 nodes. The nodes were based on significant global and local peak maxima of the seven networks derived from the ICA (see Supplementary Table S1 for exact locations of nodes). (b) Spring-embedded graphs depicting age differences in the modular organization of the brain. Graphs are based on average connectivity in each age group. Stronger segregation is reflected by higher within- and lower between-network correlations. In comparison, young adults show stronger segregation than older adults for most networks. For visualization purposes, graphs are displayed at 5% graph density. (c) Brain-wide system segregation was higher for young adults and had distinct

effects on behavior for each age group with young adults profiting from increasing segregation. (d) A different picture emerged for global efficiency, a measure of network integration. Global efficiency was calculated for individual orthogonal minimum spanning trees, which were based on weighted correlation matrices. The graphs of young adults showed stronger global efficiency than older adults. While increasing global efficiency was associated with better performance in both age groups, it predicted a slower performance in the group of young adults and a faster performance in older adults. Note that segregation and global efficiency values were mean-centered for analyses with behavior.

Brain system segregation predicts age-related differences in behavior as a function of network type

We next examined whether segregation differed between networks. Previous research showed that networks exhibit differences in their patterns of age-related changes in segregation[13]. While these studies focused on a broad distinction of sensorimotor and cognitive association networks, we investigated segregation and its behavioral relevance for each network individually to explore age-accompanied differences as a function of system type. Overall, results showed that all networks were less segregated in older than young adults (x^2= 47.06, p < 0.001; Figure 5a). However, networks' increasing segregation differed in their behavioral relevance (Table S11). For accuracy, we detected significant interactions between age and network segregation (Figure 5b) for DMN-B (x^2= 5.76, p = 0.016) and VAN-B (x^2= 18.22, p < 0.001). For response time (Figure 5c), results showed significant interactions with age and the networks DMN-A (x^2= 79.3, p < 0.001), CONT-B (x^2= 21.16, p < 0.001), and DAN-A (x^2= 68.62, p < 0.001). Overall, stronger segregation of different systems was associated with better and faster performance for young adults and poorer and slower reactions in older adults. Only increasing segregation of DMN-A predicted slower reactions in young adults which might point to a different role of this system in semantic cognition. We also explored the relationship of network segregation with neuropsychological measures (Figure 5d). Results revealed a significant positive correlation of segregation in the VAN-B with executive measures in young adults (r = 0.4, p = 0.03) and a negative correlation of DMN-B with semantic memory in older adults (r = -0.38, p = 0.045).

In summary, exploring brain system integration and segregation in a semantic task revealed age-specific dynamics where young adults clearly profit from a stronger modular network organization whereas increasing integration improves efficiency only in the aging brain.

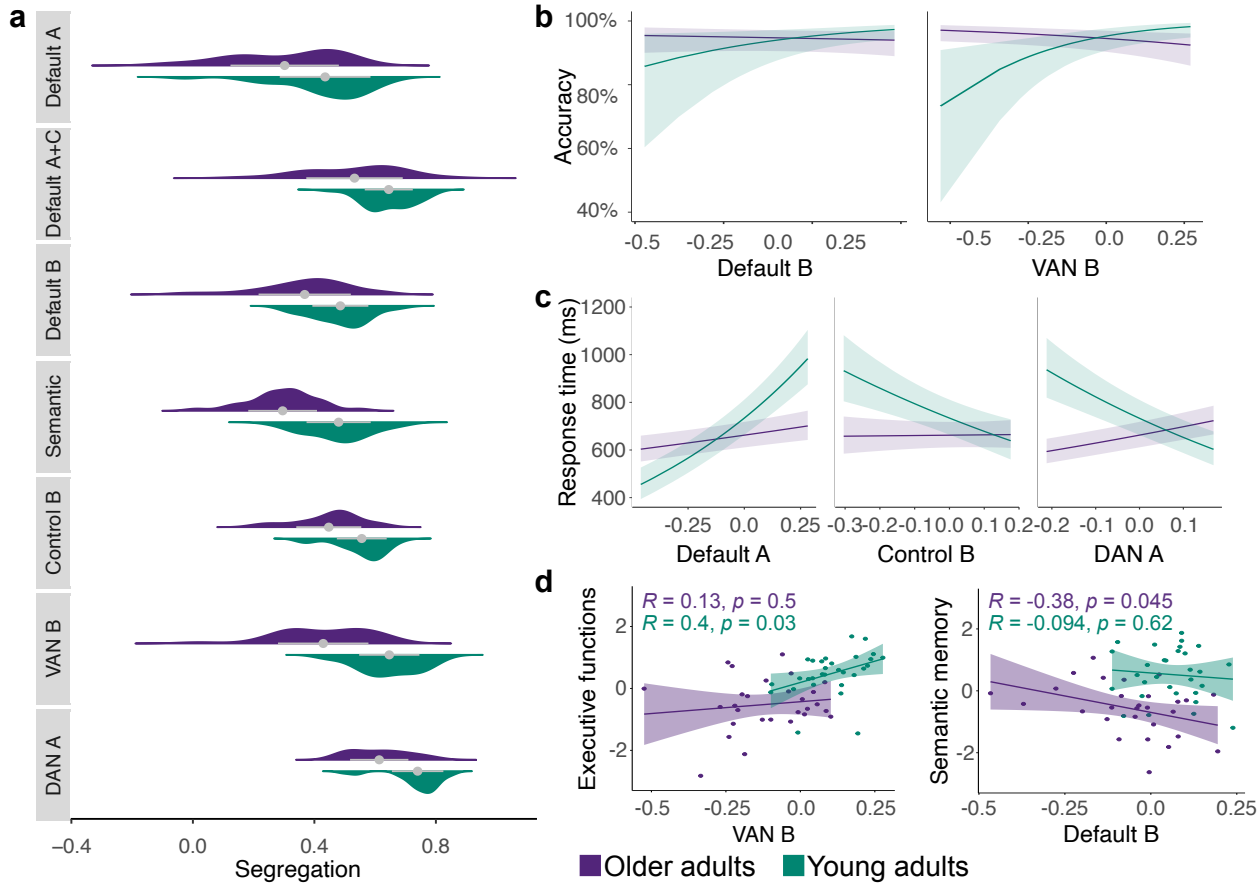

Figure 5. Segregation of individual networks is associated with distinct behavior of older and young adults as a function of system type. (a) Individual networks' segregation values by age. All networks showed stronger segregation in young adults. (b) Generalized linear mixed-effects models for accuracy revealed significant interactions with age and network segregation for two systems while (c) linear mixed-effects models for response time showed significant interactions for three networks. For most networks, increasing segregation was associated with better and faster performance in young adults and worse and slower reactions in older adults. (d) Significant correlations between network segregation and neuropsychological measures. For young adults, we detected a positive correlation of increasing segregation of VAN-B with executive functions, whereas for older adults, a negative correlation of increasing segregation of DMN-B with semantic memory was found. Note that segregation and global efficiency values were mean-centered for analyses with behavior. VAN ventral attention network, DAN dorsal attention network.

Stronger system-wide integration of brain networks in older adults is facilitated by additional connector hubs in frontal and temporal regions

An important characteristic of large-scale brain organization is the presence of regions, or nodes, that play an important role in facilitating communication between communities of a network. These nodes, commonly referred to as connector hubs, are defined by a high number of connections (edges) diversely distributed across communities[42]. Previous work has highlighted their crucial role for integrative processing in resting- and task-state networks[43]. We explored the existence of connector hubs via the normalized participation coefficient (PC)[44]. Results revealed connector hubs in bilateral frontal, parietal, and temporal regions in both age groups (Figure 6a; Table S12-13).

Notably, there were multiple nodes from the subsystems of the default network and CONT-B identified as connector hubs in the bilateral regions of the inferior parietal lobe and AG. Furthermore, both age groups had connector hubs in the right MTG and MFG. In older adults, additional connector hubs were found in the left inferior temporal gyrus and the frontal pole. A linear model revealed nodes with stronger PC only in the graphs of older adults: in the frontal pole, which was also identified as a connector hub, STG, and bilateral fusiform gyri (Figure 6b; Table S14).

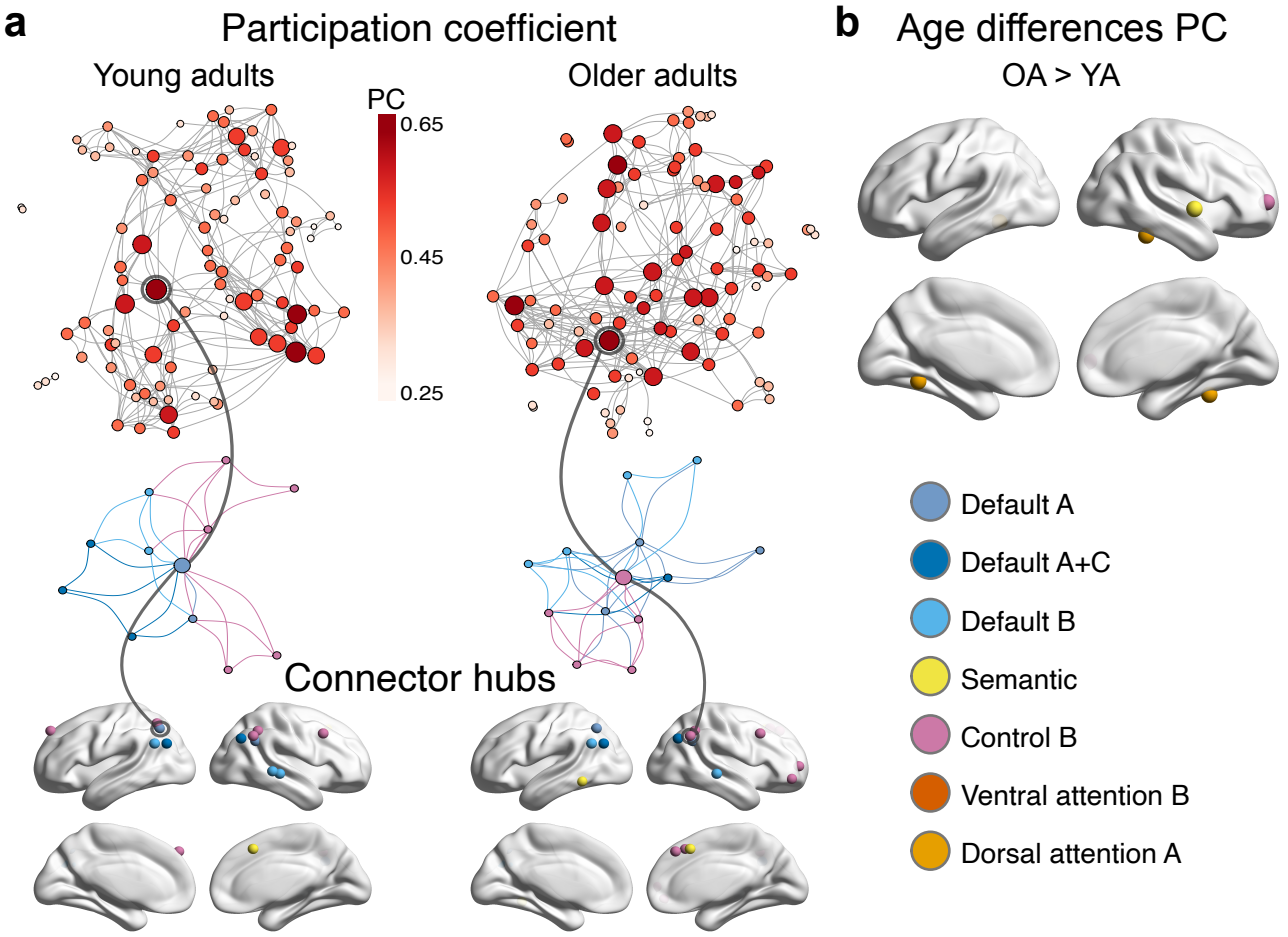

Figure 6. Topology of network hubs in young and older adults. (a) The normalized participation coefficient (PC) was calculated for individual orthogonal minimum spanning trees (OMST). Graphs display the PC of each node for the average OMST in each age group (top). For visualization purposes, the strongest 5% of connections are shown. Stronger PC values are reflected by color and node size. The higher the PC, the more a node is connected with nodes from other communities. The node with the highest PC value in each age group is extracted and displayed with its neighboring nodes colored by community (middle). Note that these connector hubs are connected to many different communities. Connector hubs were defined in each age group via PC values at least 1SD above the mean. In both groups, connector hubs were detected in frontal, parietal, and temporal regions (bottom). (b) A linear model with age as predictor revealed nodes with stronger PC only in older adults. The top and middle graphs were plotted using the ForceAtlas2 algorithm. The force-directed layout causes nodes of the same community to cluster together and diversely connected hubs (connector hubs) to appear in the center of the graph.

Discussion

The neural bases of cognitive aging remain poorly understood. It is especially debated how age-related neural reorganization impacts cognition. However, a better understanding of the neural resources that help to maintain cognitive functions and counteract decline would be mandatory to design more efficient treatment and training protocols. Previous work has largely focused on neural changes in resting-state and during processing of tasks that are primarily affected by age. In the present study, we approached this unresolved issue by investigating the functional brain organization of young and older adults in language, a key domain of human cognition that has been shown to be largely preserved in healthy aging. As a main result, we demonstrate a large-scale age-related reconfiguration of the network architecture even when older adults show intact word retrieval abilities. Overall, networks showed increased integration of task-negative and task-positive networks with age which manifested as increased coupling between functional connectivity networks, reduced segregation of global brain systems, and a larger number of connector hubs in brain graphs of older adults. Associating these age-related differences in network profiles with behavior revealed intact, albeit less efficient, performance for more integrated systems in older adults. These findings shed new light on the frequently reported pattern of declining brain system segregation with age and its impact on cognition[13,22]. Extending previous work from different cognitive domains, our results indicate a compensatory role of increased brain system integration but also reveals its limitations in terms of economical processing.

Using task-based fMRI data and group spatial ICA, we characterized seven higher-order large-scale functional networks relevant to semantic word retrieval across participants. These included default, semantic, frontoparietal control, and attention networks. Notably, our analysis detected two networks associated with semantic processing: a network component showing spatial similarity with an ALE-derived network of general semantic cognition[36] and another component overlapping with the subnetwork DMN-B[35] which has been proposed to facilitate access to semantic knowledge[1,37]. Both networks overlap in key regions of semantic processing, including left IFG, MTG, and AG. However, while the network identified as DMN-B involved bilateral ATL regions, a cross-modal hub of semantic processing[1], the semantic network component showed stronger activity in frontal regions that have been attributed to semantic control processes[36]. The semantic network component also showed strong spatial similarity with a semantic control network and a subnetwork of frontoparietal control. Thus, the networks SEM and DMN-B, which were derived in a data-driven manner for our task, appear to represent complementary aspects of semantic cognition. Moreover, in line with our previous work[29], we detected default as well as executive control and attention systems, thereby lending support to the notion that networks that have been characterized as anti-correlated during resting-state become functionally integrated for successful task processing when controlled access to semantic memory is required[45]. Indeed, exploring task-based functional connectivity within and between these networks in both age groups showed strong positive coupling

not only between subnetworks of the same system, such as the default network, but also between distinct cognitive networks. Two subnetworks of the default network, DMN-A and DMN-B, were strongly coupled with the frontoparietal control network. This finding agrees with accumulating evidence that the default network integrates with control and executive resources during goal-directed task processing[45,46], especially when complex behavior is supported by knowledge[47], and thus enables flexible cognition[37].

Our results on age-related differences in network coupling revealed additional integration of distinct networks with age. Older adults showed stronger positive coupling of SEM, CONT-B, and DAN-A with VAN-B relative to young adults, suggesting an increased cognitive demand during semantic processing. In contrast, networks of young adults displayed stronger decoupling of default systems with attention networks. Previous work indicates a modulation of network integration through task demand in young adults with more demanding cognitive functions benefiting from a more integrated brain organization to facilitate information flow across components[43,46,48]. Our results transfer this observation to the aging brain and demonstrate increased crosstalk between networks with age. Importantly, when we associated the age-related differences in network coupling with behavior, we found that enhanced coupling of different cognitive systems like default and attention networks was associated with consistently high but less efficient performance in older adults. Conversely, only increased connectivity between subsystems of the attention network predicted better and more efficient performance in young adults. Our findings offer a new perspective on the effect of a more integrated network structure in the aging brain on cognitive function. Consistent with results from the domains of working memory, episodic memory, and creative thinking[21,24,25,28], we demonstrate that enhanced integration of different cognitive systems in older adults is associated with high accuracy but at the cost of efficiency. While this network structure helps older adults to maintain cognitive flexibility, it might not be the most efficient form of wiring. These results point towards a compensatory response to age-related decline of brain function during semantic word retrieval.

We gained further insight into age differences in network architecture through the application of graph-theoretical measures. Exploring integration and segregation on a brain system level allowed us to investigate age-related changes in organization principles of task-state networks. Our results revealed global decreases in segregation and efficiency with age. The reduction of segregation in older adults is in line with previous work from resting-state[13,19,20] and task-based studies[22,24,25], as well as longitudinal investigations[16–18], and suggests that aging is associated with a reduced ability for specialized processing within highly connected clusters[10]. This was further confirmed by our results on segregation of each individual network where young adults generally showed stronger segregation.

In terms of global efficiency, the majority of resting-state and task-based studies reported lower global efficiency in older adults[18,20,49], although variability is high, and some have also

468 reported no changes or even increases with age[13,17,19,50]. These discrepancies might stem from
469 methodological considerations such as the number of nodes in a brain graph since global efficiency
470 is based on the length of its edges[51] or different thresholding methods of connectivity matrices like
471 the commonly applied proportional thresholding, which has been shown to introduce spurious
472 correlations and inflate group-related differences in graph metrics[34]. To avoid these pitfalls, our
473 calculation of global efficiency was based on the recently developed OMST[33], a data-driven
474 approach of individualized graph construction with high reliability[40,41].
475 Reduced global efficiency implies higher wiring cost and a less efficient information flow
476 among distributed networks of the global brain system[11]. This is especially relevant for the
477 processing of complex cognitive functions like semantic word retrieval which require the integration
478 of distinct networks, as revealed by our functional connectivity analyses. At the neurobiological
479 level, these changes have been associated with reduced functional connectivity of long-range
480 connections in older adults[20]. Thus, even though functional networks become more integrated with
481 age, potentially due to stronger activation of more but less specialized nodes, the efficient
482 information transfer between different networks is impaired leading to slower processing in aging.
483 This observation may represent an overall decline of cognitive attention systems in the aging brain,
484 reflected in slower responses with similar task accuracy, which was already evident at the
485 behavioral level in our data.
486 Additional evidence for this interpretation stems from the larger number of connector hubs in
487 older adults, as revealed by a higher nodal participation coefficient with age. Recent work on the
488 reconfiguration of networks from resting- to task-state in the young brain has shown an increase of
489 connector hubs with enhanced task demands to facilitate integration across different networks and
490 enable better task performance[48,52]. Moreover, studies in healthy aging have found more connector
491 hubs in older adults also during resting-state, indicating a reduced distinctiveness of network-
492 specific nodes[18,19,53]. Our work confirms these findings during task processing and allows an
493 interpretation in light of the semantic nature of our task. Nodes with a higher participation coefficient
494 in older adults were located in frontal and temporal regions and associated with CONT-B, DAN-A,
495 and SEM networks. This result underlines the enhanced cognitive demand during semantic word
496 retrieval with age and provides a mechanistic explanation for the frequently reported pattern of over-
497 activation of prefrontal control regions during demanding task processing in older adults[54]. A
498 reduced selectivity in activation of network nodes and hence an over-recruitment of less specialized
499 brain regions leads to a decline in efficient neural processing between brain regions, and this
500 process might form the basis of neural dedifferentiation in aging[18,53]. Its effect on cognition, aberrant
501 or compensatory, depends on the neurocognitive requirements of a task and an individual's neural
502 resources.
503 Exploring the topology of task-relevant neural networks as a function of cognitive
504 performance allowed us to directly link observed age-related differences with behavior. Our results

show that young adults strongly capitalized on a more segregated system during task processing, as evidenced by improved and more efficient performance during semantic word retrieval and generally better executive functions. This was true for increasing segregation on a global system level, but also for most individual networks. In contrast, increasing segregation of the whole brain graph predicted faster but not better performance in older adults. When zooming into individual networks, more segregation did not benefit older adults' behavior. Notably, enhanced segregation of DMN-B correlated negatively with semantic memory functioning in older adults, confirming the significance of this network for access to semantic memory and its necessary integration with domain-general default and executive networks for successful word retrieval in aging. Moreover, increasing global efficiency predicted better performance across groups but faster responses only in older adults. These findings have important implications for current theories on the behavioral impact of network reorganization in aging. While a less selective and more integrated network organization might not be the most efficient system in terms of processing speed, it enables older adults to maintain high performance. Consistent with previous task-based investigations[21,24,25,28], our findings thus point towards a compensatory mechanism of age-accompanied reconfiguration in network topologies. However, our results also reveal the limitations of such compensatory reorganization processes and demonstrate that a youth-like network architecture in terms of balanced integration and segregation is associated with more economical processing.

In conclusion, our findings provide evidence for age-accompanied large-scale network reorganization during access to semantic memory even when older adults show intact word retrieval abilities. In particular, functional networks of older adults were characterized by increased coupling between different systems, reduced segregation and efficiency, and a larger number of hub regions relative to young adults. Associating these changes with behavior revealed high, albeit less efficient, performance for networks in older adults showing stronger dedifferentiation and reduced distinctiveness. Our results are in line with compensatory accounts of network reconfiguration with age, but also reveal the limitations of such reorganization processes.

Methods

Participants

Participants consisted of 31 healthy older adults (mean age: 65.5 years, range: 60–69 years) and 30 healthy young adults (mean age: 27.6 years, range: 21–34 years), which is the same sample as described previously[29]. Data of three older participants as well as single runs of six participants had to be excluded due to strong motion during fMRI (>1 voxel size), leading to a final sample size of 28 participants in the older group. Inclusion criteria were native German speaker, right-handedness, normal hearing, normal or corrected-to-normal vision, no history of neurological or psychiatric conditions, and no contraindication to magnetic resonance imaging. Older adults were additionally screened for cognitive impairments with the Mini-Mental State Examination[55] (all ≥26) points and for depression with the Beck Depression Inventory[56] (all ≤14 points). A battery of neuropsychological tests was administered to assess cognitive functioning. Semantic knowledge and verbal executive functions were assessed with the German versions of the spot-the-word test (Wortschatztest)[57], the reading span test[58], and the semantic fluency test, the latter consisting of two 1-min trials of semantic categories (hobbies and surnames) that were not part of the fMRI task (Regensburger Wortflüssigkeitstest)[59]. Non-verbal executive functions were measured with the Digit Symbol Substitution Test[60] and the Trail Making Test[61]. Differences between age groups for neuropsychological measures were determined with two-sample t-tests. Prior to the experiment, participants gave written informed consent. The study was approved by the local ethics committee of the University of Leipzig and conducted in accordance with the Declaration of Helsinki.

Experimental Procedures

The experimental procedure is reported in detail in previous work[29] and briefly summarized here. Participants completed one experimental session which consisted of two runs of the fMRI experiment and neuropsychological tests, and lasted two hours in total. Experimental tasks consisted of a paced overt semantic fluency task and a control task of paced overt counting, which were implemented in a block design in the scanner (Figure 1 in Results). For the semantic fluency task, participants were asked to produce exemplars for 20 semantic categories, which were divided in 10 easy (e.g., colors) and 10 difficult (e.g., insects) categories based on a separate pilot study in healthy young and older adults[29]. Task blocks were 43 s long and separated by rest blocks of 16 s. Each block started with a 2 s visual word cue indicating whether participants were expected to generate category exemplars or count forward (1 to 9) or backward (9 to 1). This was followed by nine consecutive trials of the same category or counting task, respectively. Trials within one block were separated by inter-stimulus intervals of 2-4 s. Participants were instructed to generate one exemplar for a category or one number per trial, which was indicated by a green cross on the screen, and to pause when the cross turned red. They were told not to repeat items and to say

568 “next” if they could not think of an exemplar for the respective category. Each run contained 10
569 semantic fluency blocks, divided in easy and difficult categories, and 10 counting blocks, consisting
570 of forward and backward counting, thus resulting in a total duration of 19.4 min per run. The order of
571 blocks was counter-balanced and pseudo-randomized across participants. Before the fMRI
572 experiment, participants received instructions and practiced the task with a separate set of
573 categories outside the scanner. Stimuli were presented using the software Presentation
574 (Neurobehavioral Systems, Berkeley, USA; version 18.0). Answers were recorded via a FOMRI III
575 microphone (Optoacoustics, Yehuda, Israel). After the experiment, response recordings were
576 analyzed for verbal answers and onset times after being cleaned from scanner noise via Audacity
577 software (version 2.3.2) and transcribed by three independent raters.

578

579 **fMRI Data Acquisition and Preprocessing**

580 fMRI data were collected on a 3 T Prisma scanner (Siemens, Erlangen, Germany) with a 32-
581 channel head coil. For the acquisition of functional images, a multiband dual gradient-echo echo-
582 planar imaging sequence was used for optimal blood oxygenation level-dependent (BOLD)
583 sensitivity throughout the entire brain[1,2]. The following scanning parameters were applied: TR =
584 2000 ms; TE = 12 ms, 33 ms; flip angle = 90°; voxel size = 2.5 x 2.5 x 2.75 mm with an inter-slice
585 gap of 0.25 mm; FOV = 204 mm; multiband acceleration factor = 2. To increase coverage of
586 anterior temporal lobe (ATL) regions, slices were tilted by 10° of the AC-PC line. 616 images
587 consisting of 60 axial slices in interleaved order covering the whole brain were continuously
588 acquired per run. Additionally, field maps were obtained for later distortion correction (TR = 8000
589 ms; TE = 50 ms). This study analyzed the data from echo 2 (TE = 33 ms) since preprocessing was
590 performed using the software fMRIPrep[3], which currently does not support the combination of
591 images acquired at different echo times. We chose to use results from preprocessing with fMRIPrep
592 since this pipeline provides state-of-the-art data processing while allowing for full transparency and
593 reproducibility of the applied methods and a comprehensive quality assessment of each processing
594 step that facilitates the identification of potential outliers. We also double-checked results from
595 preprocessing with fMRIPrep with a conventional SPM preprocessing pipeline of both echoes. The
596 comparison of both pipelines did not reveal big differences in analysis results. A high-resolution, T1-
597 weighted 3D volume was obtained from our in-house database (if it was not older than two years) or
598 collected after the functional scans using an MPRAGE sequence (176 slices in sagittal orientation;
599 TR = 2300 ms; TE = 2.98 ms; flip angle = 9°; voxel size = 1 x 1 x 1 mm; no slice gap; FOV = 256
600 mm). Preprocessing was performed using fMRIPprep 20.2.3[3] which is based on Nipype 1.6.1[4]. In
601 short, preprocessing steps included skull stripping, distortion correction, co-registration, slice timing
602 correction, and calculation of several confounding time-series for each of the two BOLD runs per
603 participant. Anatomical T1-weighted images were skull-stripped, segmented, and spatially

normalized. For spatial normalization to standard space, the Montreal Neurological Institute (MNI) ICBM 152 non-linear 6th Generation Asymmetric Average Brain Stereotaxic Registration Model (MNI152NLin6Asym) was entered as output space in fMRIPrep. For more details on the preprocessing pipeline, see the section corresponding to workflows in fMRIPrep's documentation (https://fmriprep.org/en/20.2.3/workflows.html). After preprocessing, 29 volumes from the beginning of each run were discarded since they were collected for the combination of the short and long TE images. This yielded 587 normalized images per run which were included in further analyses.

Independent component analysis

We applied group-wise ICA to define spatially independent task-active networks in a data-driven manner. ICA has been shown to decompose fMRI time series into reliable functionally connected components with the advantage of simultaneously removing non-neural fluctuations through the identification of artefactual components[64]. Preprocessed, normalized data were smoothed with a 5 mm^3 FWHM Gaussian kernel and entered into a general linear model for each participant and session using Statistical Parametrical Mapping software (SPM12; Wellcome Trust Centre for Neuroimaging), implemented in MATLAB (version 9.10/R2021a). GLMs included regressors for the task blocks (semantic fluency and counting) as well as nuisance regressors consisting of the six motion parameters and individual regressors for strong volume-to-volume movement as indicated by values of framewise displacement > 0.9[65]. Additionally, an individual regressor of no interest was included in the design matrix if a participant had missed a whole task block during the experiment (n = 10). Before model estimation, a high-pass filter with a cut-off at 128 s was applied to the data.

Preprocessed, normalized and smoothed data were analyzed using the Group ICA of fMRI Toolbox (GIFT v4.0c). Dimensions were reduced to 55 using minimum description length information criteria. Icasso was repeated 50 times to ensure reliability of the decomposition, and group-level ICs were back-reconstructed to the participant level using the group-information guided ICA (GICA3) algorithm[66]. We calculated group ICA treating all participants as one group to ensure that the same components were identified in both groups. We discarded those components related to banding artifacts and noise after careful visual inspection of the spatial maps according to established criteria[64] (see Supplementary Figure S1 for an overview of all 55 ICs). Of the remaining 13 non-noise components, seven components of interest were selected. To characterize the spatial extent of the seven remaining components at the group level, we calculated one-sided t-tests for participants' spatial maps. A gray matter mask that restricted statistical tests to voxels in the cerebrum was applied to all group-level analyses. Results were corrected for multiple comparisons using a peak level threshold at $p < 0.05$ with the family-wise error (FWE) method and a cluster-extent threshold of 10 voxels.

Brain network construction

Brain networks were constructed based on the seven selected component maps of the ICA. To determine network labeling of the thresholded maps, we used the Jaccard index (*J*), a measure of spatial similarity[67]. By calculating the ratio of overlapping voxels in two binary spatial network maps relative to all active voxels in either image, the Jaccard index can be used as a measure to assess the fit between a spatial component map (*A*) and a template image (*B*):

$$J = \frac{|A \cap B|}{|A \cup B|}$$

The index ranges from 0 to 1, with a high Jaccard index denoting high similarity of two spatial maps. It has been used previously to assess similarity of brain activation maps with template network parcellations[68,69]. We defined a minimum threshold of J = 0.15 to consider a network template for a spatial component mask[69]. Next, if two components were best described by the same network template thereby indicating that the network might have split up in multiple components, we assessed the similarity of the combined component maps to the template. If the combined map reached a higher similarity index than each component individually, the combination was kept as a reflection of the respective network.

As template masks, we used the 17-networks functional connectivity-based parcellation scheme[35] as well as the network masks of general semantic cognition and semantic control defined in a meta-analysis[36]. We included separate template masks for semantic cognition in our analysis to account for the semantic nature of our task. We also probed similarity of Jaccard indices with a 7-networks parcellation scheme[35]. While the results for the 7-networks parcellation generally agreed with the more fine-grained parcellation, the 7-networks parcellation resulted in three components showing high spatial similarity with the default network template. However, differential roles have been reported for subsystems of the default network when access to semantic memory is required[6]. Specifically, the dorsal medial subsystem of the default network ("Default B" in the 17-networks parcellation scheme) has been shown to broadly overlap with a left-lateralized temporal-frontal semantic network[6,7]. Since we were interested in the age-dependent interplay of domain-specific and domain-general networks in semantic cognition, the remaining analyses were based on the 17-networks parcellation scheme.

Based on the results of the Jaccard index, each thresholded component map was inclusively masked by the respective resampled template network. We were interested in the effect of age on the functional connectivity within and between selected networks. In a first step, to explore functional connectivity between networks, we extracted averaged time series across all voxels within one masked component, thus leading to seven time series per participant and run. Second, networks were further parcellated into distinct regions of interest (ROIs) based on peak maxima of activated clusters. ROIs were created for all peak maxima of a significant cluster (up to three ROIs

675 per cluster) using the MarsBar toolbox[70]. To this end, identified clusters were extracted from the
676 thresholded and masked component maps, spheres of 5 mm surrounding each maximum
677 coordinate were created, and, in a last step, both images were combined. In this way, we ensured
678 that ROIs would only contain voxels that were included in the group-level statistics. Parcellating the
679 seven network components based on strongest correlation peaks led to 126 cortical ROIs per
680 participant and run.
681 Functional time series were extracted for the seven ROIs and 126 ROIs parcellation
682 schemes from non-smoothed functional data. To account for motion artifacts and other signal
683 confounds, the following denoising pipeline was applied during time series extraction: 24
684 realignment parameters (six motion parameters, temporal derivatives, and quadratic terms), global
685 signal, and top five aCompCor components for white matter and cerebral spinal fluid, respectively.
686 Censoring included a framewise displacement threshold of 0.9 mm and 18 discrete cosine-basis
687 regressors to account for signal drifts. All these regressors were combined in a design matrix and
688 removed from the data in a single step[71,72]. The denoising strategy was based on recent
689 recommendations[73] that compared the performance of different denoising pipelines for analysis of
690 task-based functional connectivity. Consistent with previous research on resting-state functional
691 connectivity[74,75], the authors reported that the inclusion of global signal in a denoising pipeline
692 markedly reduced global motion artifacts and led to more comparable results across conditions in
693 task-based functional connectivity data[73]. Further, time series were detrended and demeaned, and
694 functional images were masked with a subject-specific, resampled gray matter mask before
695 denoising. During signal extraction for the set of 126 ROIs, the number of voxels per ROI and
696 participant were extracted. ROIs for which more than 15% of participants did not show any signal
697 coverage were excluded. The resulting 121 ROIs were used for the remaining analyses.

698

699 **Functional connectivity matrices**

700 We applied cPPI analyses[38] to obtain connectivity terms that describe task-related interactions
701 between our networks and regions of interest. In contrast to traditional PPI analyses, cPPI results in
702 undirected, symmetrical connectivity matrices that are based on pairwise partial correlations
703 between ROIs. We calculated cPPI for our contrast of interest semantic fluency > counting,
704 separately for the 7-networks and 121-ROIs parcellations. In brief, the deconvolved time series for
705 each ROI was multiplied with the task time course from the first-level GLM design matrix and
706 convolved with a canonical HRF to form a PPI term. Pairwise partial correlations were estimated
707 between PPI terms of two regions while controlling for the observed BOLD signal in both regions,
708 the original task regressor and average in-scanner head motion (mean FD). Connectivity matrices
709 were calculated for each run separately and then averaged, resulting in a 7 x 7 and 121 x 121

correlation matrix per participant. Subsequently, correlation coefficients were Fisher-transformed to z values.

Network measures

Within- and between-network functional connectivity

Within- and between-network functional connectivity were explored for the 7-networks and 121-ROIs connectivity matrices in both age groups. Using the connectivity matrices with seven networks allowed us to investigate the coupling and decoupling between task-relevant networks while the more fine-grained parcellation provided additional insights into the coupling of regions within distinct networks. All subsequent network measures were based on the 121-ROIs connectivity matrices.

Brain system segregation

We calculated global segregation as previously implemented by Chan and colleagues[9,13,76], using the unthresholded, weighted connectivity matrices. In line with previous work on functional connectivity in healthy aging[18,76], we excluded negative correlations from segregation and integration analyses by setting them to zero. Excluding negative correlations has been shown to improve the reliability of graph measures[77] and to help avoid interpretational difficulty, for example when it comes to concepts like shortest paths[78]. Building upon the network parcellation of our ICA analysis, each functional network was treated as a distinct system, and segregation was computed as the difference between mean within-system ($\overline{Z}_w$) and mean between-system ($\overline{Z}_b$) correlations divided by mean within-system correlation as shown in the following equation:

$$\text{Brain system segregation} = \frac{\overline{Z}_w - \overline{Z}_b}{\overline{Z}_w}$$

A higher ratio score denotes greater separation of functional systems.

We also calculated segregation values for each functional network individually such that within-system connectivity $\overline{Z}_w$ represents the mean of all edges (correlations) between pairwise nodes that belong to the same network and between-system connectivity $\overline{Z}_b$ reflects the mean of all edges between nodes of the respective network and all other nodes.

Edge filtering

Most graph theoretical measures require some form of filtering to obtain a sparse graph that is more likely to represent true functional connectivity than a maximally dense graph as produced by a correlation matrix[78]. While threshold-based filtering methods like proportional or absolute thresholding are commonly applied in network neuroscience, they are driven by an arbitrary choice of the respective threshold and suffer from low reliability[40]. To avoid these pitfalls and based on recent research on the reliability of graph construction in neuroscience[40,41], we calculated the

745 orthogonalized minimum spanning tree (OMST)[33] on the weighted functional connectivity matrices.
746 Apart from its high reliability, the OMST has several advantages compared to commonly applied
747 threshold-based methods of graph construction: It adheres to the intrinsic topological structure of
748 the brain network by resulting in a fully connected, weighted graph and offers a data-driven method
749 of individualized network construction accounting for each individual's optimal state of economic
750 wiring in terms of cost and efficiency. In contrast to the original minimum spanning tree (MST), the
751 OMST filters connectivity networks until the highest global cost efficiency (GCE) of a graph is
752 reached while including both strong and weak connections and preserving the same mean degree
753 across groups.
754 The OMST was calculated in three steps as described by Dimitriadis et al. (2017): (a) the
755 MST of a graph is defined; (b) the corresponding edges of the MST are removed from the original
756 graph by setting edge weights to 0; (c) steps (a) and (b) are repeated until the GCE of the graph is
757 optimized. GCE is defined as the global efficiency minus cost, where cost corresponds to the total
758 weights of the selected edges of the OMST divided by the sum of the edges of the original fully
759 weighted graph[12]. The final OMST is constructed by combining all the removed, non-overlapping
760 MSTs. To show that the OMST indeed results in higher GCE than other filtering methods, we
761 compared the GCE for OMST, MST, and a method of proportional thresholding where we used a
762 common range of 5-20% strongest edge weights of a graph (Supplementary Figure S3). To avoid
763 differences in graph measures caused by the number of nodes in a graph, we excluded all nodes
764 where at least one participant had no signal during construction of matrices. This resulted in a
765 104x104 matrix per participant, which was used for construction of OMST and all subsequent
766 measures.
767
768 *Brain system integration*
769 We calculated global efficiency as a measure of system-wide integration. It is defined as the
770 average of the inverse shortest path length between all pairs of nodes in a graph and is thus a
771 measure of efficient signal transmission[10,39].

772 $$\text{Global efficiency} = \frac{1}{N(N-1)} \sum_{i \neq j \in G} \frac{1}{L_{i,j}}$$

773 Global efficiency was based on the individual OMSTs using the reciprocal edge weights to obtain a
774 distance matrix where high weights signify short paths between nodes.
775
776 *Global network hubs*
777 We identified hubs via the normalized participation coefficient (PC)[44]. The PC provides insight into
778 the functional role of a node. Specifically, it evaluates whether a node mainly interacts with nodes
779 from its community or multiple communities of a network[79]. In network neuroscience, PC has been
780 applied to define nodes that are important for communication between communities (connector

hubs) and nodes that are central to the communication within communities (provincial hubs)[42,43,52]. Recently, it has been shown that the conventional measure of PC is strongly influenced by the size and connectedness of its community leading to a reduced interpretational value of this graph measure[44]. Thus, a normalized version of the PC has been introduced that accounts for these differences in real-world networks while preserving its meaning. It is calculated similarly to the original PC as one minus the ratio between the degree k of node i with nodes in its community m and the degree of node i with all other nodes in the network. However, a normalization factor is added by subtracting the median degree of this node in a series of random networks:

$$\text{Normalized PC} = 1 - \sqrt{B_0 \sum_{m \in M} \left(\frac{k_i(m) - k_i(m)_{rand}}{k_i} \right)^2}$$

We calculated 100 random networks for each node. Connector hubs were then defined as nodes with a PC value of at least 1SD above the mean in each age group.

Statistical analysis

Age-related changes for within- and between-network functional connectivity

To assess differences between age groups for within- and between-network connectivity, we ran two-sample t-tests for each edge of the 7-network and 121-ROIs connectivity matrices within the Network-Based Statistics toolbox (NBS)[51]. NBS applies cluster-based thresholding to correct for multiple comparisons using permutation testing. In contrast to more conventional procedures for controlling the family-wise error rate, such as the false discovery rate, NBS considers connected components in networks (graphs), which makes it especially suited for network statistics. We set an initial cluster-forming threshold at $p < 0.01$ (two-sided test; $t = 2.67$) and an FWE-corrected significance threshold at $p < 0.05$ with 10,000 permutations. To control for the influence of motion on functional connectivity, the average in-scanner head motion per participant was included as a covariate. Average head motion was defined as the mean FD based on the calculation of the root mean square deviation of the relative transformation matrices[80].

Age-related changes for network measures of segregation and integration

Linear mixed-effects models were set up to examine how the dependent variables brain system segregation, individual network segregation, global efficiency, and nodal participation coefficient were predicted by age group. We included in-scanner head motion (mean FD) as covariate and a random intercept for participants. Models were calculated as follows:

$$\text{Network measure} = \beta_0 + \beta_1 \text{Age} + \beta_2 \text{Motion} + (1|\text{Subject}) + \varepsilon$$

Significance values were obtained by likelihood ratio tests of the full model with the effect in question against the model without the effect in question.

Association between network measures and cognitive performance

For those network measures that showed differences between young and older adults, we further examined their association with participants' cognitive performance for the in-scanner task and the neuropsychological test battery. Analyses were performed using mixed-effects models with a logistic regression for accuracy data due to their binomial nature and a linear regression for log-transformed response time data. We only analyzed response times for correct reactions for the semantic fluency task since our connectivity values were also based on our contrast of interest semantic fluency > counting. Models contained fixed effects for the respective mean-centered network measure (between-network functional connectivity, brain system segregation, individual network segregation, and global efficiency) and age group as well as their interaction term, and random intercepts for participants and semantic categories. Further, mean-centered values of mean FD and education were entered as covariates. Models were set up as shown in the following equation:

$$\text{Cognitive measure} = \beta_0 + \beta_1\text{Network measure} + \beta_2\text{Age} + \beta_3\text{Network measure} \times \text{Age} + \beta_4\text{Motion} + \beta_5\text{Education} + (1|\text{Subject}) + (1|\text{Category}) + \varepsilon$$

where cognitive measure denotes accuracy and response time, respectively. Significance values were obtained via likelihood ratio tests. We applied sum coding (ANOVA-style encoding) for all categorical predictors.

We performed correlation analyses with the neuropsychological tests that had been assessed outside of the scanner. Due to the collinearity of some neuropsychological tests, we ran an exploratory factor analysis on the standardized test scores using maximum likelihood estimation and varimax rotation. Based on the hypothesis test (χ^2 = 14.04, p = 0.081), two factors with an eigenvalue > 1 were chosen. For subsequent correlations with network measures, participant factor scores extracted via regression methods were used.

All statistical models except for NBS were performed using R 4.1.0 via RStudio[81] and the package lme4[82]. Results were visualized using the ggplot2[83] and ggeffects[84] packages. If applicable, post-hoc comparisons were applied using the package emmeans[85]. The exploratory factor analysis was calculated with the stats package[81]. OMSTs and all graph theory measures were calculated in Matlab using the Brain Connectivity toolbox[10] and publicly available scripts for OMST and normalized PC. Chord diagrams were generated with the circlize package[86], spring-embedded plots using the igraph package[87], and force-directed plots using the ForceAtlas2 algorithm for R available on Github (https://github.com/analyxcompany/ForceAtlas2).

Data availability

All behavioral data and raw data of functional connectivity and graph-theoretical measures are available in a public repository at https://gitlab.gwdg.de/functionalconnectivityaging/mdn_lang_networkAnalysis. This repository also holds all self-written code for analyses and figures for this project. Raw neuroimaging data are protected under the General Data Protection Regulation (EU) and can only be made available from the authors upon reasonable request.

Acknowledgments

The authors would like to thank the medical technical assistants of MPI CBS for their support with data acquisition, and Annika Dunau, Caroline Duchow, and Rebekka Luckner for their support with transcriptions of recordings.

Author contributions

S.M. collected, processed, and analyzed the data. K.A.W. contributed to analyses. D.S. contributed to the interpretation of results and the writing of the manuscript. S.M. and G.H. interpreted the results and wrote the paper.

Funding

SM held a stipend by the German Academic Scholarship Foundation (Studienstiftung des deutschen Volkes). DS was supported by the Deutsche Forschungsgemeinschaft (SA 1723/5-1) and the James S. McDonnell Foundation (Understanding Human Cognition, #220020292). GH was supported by the Lise Meitner excellence program of the Max Planck Society and the Deutsche Forschungsgemeinschaft (HA 6314/3-1, HA 6314/4-1).

Competing Interests

The authors declare that no competing interests exist.

References

1. Lambon Ralph, M. A., Jefferies, E., Patterson, K. & Rogers, T. T. The neural and computational bases of semantic cognition. *Nat. Rev. Neurosci.* **18**, 42–55 (2017).
2. Nilsson, L.-G. Memory function in normal aging. *Acta Neurol. Scand. Suppl.* **179**, 7–13 (2003).
3. Nyberg, L., Backman, L., Erngrund, K., Olofsson, U. & Nilsson, L.-G. Age Differences in Episodic Memory, Semantic Memory, and Priming: Relationships to Demographic, Intellectual, and Biological Factors. *J. Gerontol. B. Psychol. Sci. Soc. Sci.* **51B**, P234–P240 (1996).
4. Verhaegen, P., Borchelt, M. & Smith, J. Relation Between Cardiovascular and Metabolic Disease and Cognition in Very Old Age: Cross-Sectional and Longitudinal Findings From the Berlin Aging Study. *Health Psychol.* **22**, 559–569 (2003).
5. Burke, D. M. & Shafto, M. A. Aging and Language Production. *Curr. Dir. Psychol. Sci.* **13**, 21 (2004).
6. Hedden, T. & Gabrieli, J. D. E. Insights into the ageing mind: a view from cognitive neuroscience. *Nat. Rev. Neurosci.* **5**, 87–96 (2004).
7. Meunier, D., Lambiotte, R., Fornito, A., Ersche, K. & Bullmore, E. Hierarchical modularity in human brain functional networks. *Front. Neuroinformatics* **3**, (2009).
8. Power, J. D. *et al.* Functional Network Organization of the Human Brain. *Neuron* **72**, 665–678 (2011).
9. Wig, G. S. Segregated Systems of Human Brain Networks. *Trends Cogn. Sci.* **21**, 981–996 (2017).
10. Rubinov, M. & Sporns, O. Complex network measures of brain connectivity: Uses and interpretations. *NeuroImage* **52**, 1059–1069 (2010).
11. Bullmore, E. & Sporns, O. The economy of brain network organization. *Nat. Rev. Neurosci.* **13**, 336–349 (2012).
12. Bassett, D. S. *et al.* Cognitive fitness of cost-efficient brain functional networks. *Proc. Natl. Acad. Sci.* **106**, 11747–11752 (2009).
13. Chan, M. Y., Park, D. C., Savalia, N. K., Petersen, S. E. & Wig, G. S. Decreased segregation of brain systems across the healthy adult lifespan. *Proc. Natl. Acad. Sci.* **111**, E4997–E5006 (2014).
14. Setton, R. *et al.* Age differences in the functional architecture of the human brain. *Cereb. Cortex* bhac056 (2022) doi:10.1093/cercor/bhac056.
15. Stumme, J., Jockwitz, C., Hoffstaedter, F., Amunts, K. & Caspers, S. Functional network reorganization in older adults: Graph-theoretical analyses of age, cognition and sex. *NeuroImage* **214**, 116756 (2020).
16. Betzel, R. F. *et al.* Changes in structural and functional connectivity among resting-state networks across the human lifespan. *NeuroImage* **102**, 345–357 (2014).
17. Cao, M. *et al.* Topological organization of the human brain functional connectome across the lifespan. *Dev. Cogn. Neurosci.* **7**, 76–93 (2014).
18. Chong, J. S. X. *et al.* Longitudinal Changes in the Cerebral Cortex Functional Organization of Healthy Elderly. *J. Neurosci.* **39**, 5534–5550 (2019).
19. Geerligs, L., Renken, R. J., Saliasi, E., Maurits, N. M. & Lorist, M. M. A Brain-Wide Study of Age-Related Changes in Functional Connectivity. *Cereb. Cortex* **25**, 1987–1999 (2015).
20. Sala-Llonch, R. *et al.* Changes in whole-brain functional networks and memory performance in aging. *Neurobiol. Aging* **35**, 2193–2202 (2014).
21. Deng, L. *et al.* Age-Related Compensatory Reconfiguration of PFC Connections during Episodic Memory Retrieval. *Cereb. Cortex* **31**, 717–730 (2021).

22. Geerligs, L., Maurits, N. M., Renken, R. J. & Lorist, M. M. Reduced specificity of functional connectivity in the aging brain during task performance. *Hum. Brain Mapp.* **35**, 319–330 (2014).
23. Spreng, R. N., Stevens, W. D., Viviano, J. D. & Schacter, D. L. Attenuated anticorrelation between the default and dorsal attention networks with aging: evidence from task and rest. *Neurobiol. Aging* **45**, 149–160 (2016).
24. Crowell, C. A. *et al.* Older adults benefit from more widespread brain network integration during working memory. *NeuroImage* **218**, 116959 (2020).
25. Gallen, C. L., Turner, G. R., Adnan, A. & D'Esposito, M. Reconfiguration of brain network architecture to support executive control in aging. *Neurobiol. Aging* **44**, 42–52 (2016).
26. Capogna, E. *et al.* Whole-brain connectivity during encoding: age-related differences and associations with cognitive and brain structural decline. *Cereb. Cortex* bhac053 (2022) doi:10.1093/cercor/bhac053.
27. Pongpipat, E. E., Kennedy, K. M., Foster, C. M., Boylan, M. A. & Rodrigue, K. M. Functional Connectivity Within and Between n-Back Modulated Regions: An Adult Lifespan Psychophysiological Interaction Investigation. *Brain Connect.* **11**, 103–118 (2021).
28. Adnan, A., Beaty, R., Silvia, P., Spreng, R. N. & Turner, G. R. Creative aging: functional brain networks associated with divergent thinking in older and younger adults. *Neurobiol. Aging* **75**, 150–158 (2019).
29. Martin, S., Saur, D. & Hartwigsen, G. Age-Dependent Contribution of Domain-General Networks to Semantic Cognition. *Cereb. Cortex* **32**, 870–890 (2022).
30. Gordon, J., Young, M. & Garcia, C. Why do older adults have difficulty with semantic fluency? *Aging Neuropsychol. Cogn.* **25**, 803–828 (2018).
31. Ferré, P., Jarret, J., Brambati, S. M., Bellec, P. & Joanette, Y. Task-Induced Functional Connectivity of Picture Naming in Healthy Aging: The Impacts of Age and Task Complexity. *Neurobiol. Lang.* 1–24 (2020) doi:10.1162/nol_a_00007.
32. Marsolais, Y., Perlbarg, V., Benali, H. & Joanette, Y. Age-related changes in functional network connectivity associated with high levels of verbal fluency performance. *Cortex* **58**, 123–138 (2014).
33. Dimitriadis, S. I., Salis, C., Tarnanas, I. & Linden, D. E. Topological Filtering of Dynamic Functional Brain Networks Unfolds Informative Chronnectomics: A Novel Data-Driven Thresholding Scheme Based on Orthogonal Minimal Spanning Trees (OMSTs). *Front. Neuroinformatics* **11**, (2017).
34. van den Heuvel, M. P. *et al.* Proportional thresholding in resting-state fMRI functional connectivity networks and consequences for patient-control connectome studies: Issues and recommendations. *NeuroImage* **152**, 437–449 (2017).
35. Yeo, B. T. *et al.* The organization of the human cerebral cortex estimated by intrinsic functional connectivity. *J. Neurophysiol.* **106**, 1125–1165 (2011).
36. Jackson, R. L. The neural correlates of semantic control revisited. *NeuroImage* **224**, 117444 (2021).
37. Smallwood, J. *et al.* The default mode network in cognition: a topographical perspective. *Nat. Rev. Neurosci.* **22**, 503–513 (2021).
38. Fornito, A., Harrison, B. J., Zalesky, A. & Simons, J. S. Competitive and cooperative dynamics of large-scale brain functional networks supporting recollection. *Proc. Natl. Acad. Sci.* **109**, 12788–12793 (2012).
39. Latora, V. & Marchiori, M. Efficient Behavior of Small-World Networks. *Phys. Rev. Lett.* **87**, 198701 (2001).
40. Luppi, A. I. & Stamatakis, E. A. Combining network topology and information theory to construct representative brain networks. *Netw. Neurosci.* **5**, 96–124 (2021).

41. Jiang, C. *et al.* Toward Reliable Network Neuroscience for Mapping Individual Differences. 2021.05.06.442886 (2021) doi:10.1101/2021.05.06.442886.
42. Bertolero, M. A., Yeo, B. T. T. & D'Esposito, M. The diverse club. *Nat. Commun.* **8**, 1277 (2017).
43. Cohen, J. R. & D'Esposito, M. The Segregation and Integration of Distinct Brain Networks and Their Relationship to Cognition. *J. Neurosci.* **36**, 12083–12094 (2016).
44. Pedersen, M., Omidvarnia, A., Shine, J. M., Jackson, G. D. & Zalesky, A. Reducing the influence of intramodular connectivity in participation coefficient. *Netw. Neurosci.* **4**, 416–431 (2020).
45. Krieger-Redwood, K. *et al.* Down but not out in posterior cingulate cortex: Deactivation yet functional coupling with prefrontal cortex during demanding semantic cognition. *NeuroImage* **141**, 366–377 (2016).
46. Vatansever, D., Menon, D. K., Manktelow, A. E., Sahakian, B. J. & Stamatakis, E. A. Default Mode Dynamics for Global Functional Integration. *J. Neurosci.* **35**, 15254–15262 (2015).
47. Wang, X., Gao, Z., Smallwood, J. & Jefferies, E. Both Default and Multiple-Demand Regions Represent Semantic Goal Information. *J. Neurosci.* **41**, 3679–3691 (2021).
48. Zhang, W., Tang, F., Zhou, X. & Li, H. Dynamic Reconfiguration of Functional Topology in Human Brain Networks: From Resting to Task States. *Neural Plast.* **2020**, 8837615 (2020).
49. Gonzalez-Burgos, L. *et al.* Cortical Networks Underpinning Compensation of Verbal Fluency in Normal Aging. *Cereb. Cortex* **31**, 3832–3845 (2021).
50. Song, J. *et al.* Age-Related Reorganizational Changes in Modularity and Functional Connectivity of Human Brain Networks. *Brain Connect.* **4**, 662–676 (2014).
51. Zalesky, A., Fornito, A. & Bullmore, E. T. Network-based statistic: Identifying differences in brain networks. *NeuroImage* **53**, 1197–1207 (2010).
52. Bertolero, M. A., Yeo, B. T. T., Bassett, D. S. & D'Esposito, M. A mechanistic model of connector hubs, modularity and cognition. *Nat. Hum. Behav.* **2**, 765–777 (2018).
53. Chan, M. Y., Alhazmi, F. H., Park, D. C., Savalia, N. K. & Wig, G. S. Resting-State Network Topology Differentiates Task Signals across the Adult Life Span. *J. Neurosci.* **37**, 2734–2745 (2017).
54. Davis, S. W., Dennis, N. A., Daselaar, S. M., Fleck, M. S. & Cabeza, R. Que PASA? The Posterior-Anterior Shift in Aging. *Cereb. Cortex* **18**, 1201–1209 (2008).
55. Folstein, M. F., Folstein, S. E. & McHugh, P. R. "Mini-mental state": A practical method for grading the cognitive state of patients for the clinician. *J. Psychiatr. Res.* **12**, 189–198 (1975).
56. Beck, A. T., Steer, R. A., Ball, R. & Ranieri, W. Comparison of Beck Depression Inventories -IA and -II in psychiatric outpatients. *J. Pers. Assess.* **67**, 588–597 (1996).
57. Schmidt, K.-H. & Metzler, P. *WST-Wortschatztest*. (Beltz Test, 1992).
58. Daneman, M. & Carpenter, P. A. Individual differences in working memory and reading. *J. Verbal Learn. Verbal Behav.* **19**, 450–466 (1980).
59. Aschenbrenner, S., Tucha, O. & Lange, K. W. *Regensburger Wortflüssigkeits-Test*. (Hogrefe, 2000).
60. Wechsler, D. *The measurement of adult intelligence (3rd ed.).* (Williams & Wilkins Co, 1944). doi:10.1037/11329-000.
61. Reitan, R. M. Validity of the Trail Making Test as an indicator of organic brain damage. *Percept. Mot. Skills* **8**, 271 (1958).
62. Esteban, O. *et al.* fMRIPrep: a robust preprocessing pipeline for functional MRI. *Nat. Methods* **16**, 111–116 (2019).
63. Gorgolewski, K. *et al.* Nipype: A Flexible, Lightweight and Extensible Neuroimaging Data Processing Framework in Python. *Front. Neuroinformatics* **5**, 13 (2011).

64. Griffanti, L. *et al.* ICA-based artefact and accelerated fMRI acquisition for improved Resting State Network imaging. *NeuroImage* **95**, 232–247 (2014).
65. Siegel, J. S. *et al.* Statistical improvements in functional magnetic resonance imaging analyses produced by censoring high-motion data points. *Hum. Brain Mapp.* **35**, 1981–1996 (2014).
66. Calhoun, V. D., Adali, T., Pearlson, G. D. & Pekar, J. J. A method for making group inferences from functional MRI data using independent component analysis. *Hum. Brain Mapp.* **14**, 140–151 (2001).
67. Jaccard, P. The Distribution of the Flora in the Alpine Zone. *New Phytol.* **11**, 37–50 (1912).
68. Gordon, E. M. *et al.* Default-mode network streams for coupling to language and control systems. *Proc. Natl. Acad. Sci.* (2020) doi:10.1073/pnas.2005238117.
69. Jackson, R. L., Cloutman, L. L. & Lambon Ralph, M. A. Exploring distinct default mode and semantic networks using a systematic ICA approach. *Cortex* **113**, 279–297 (2019).
70. Brett, M., Anton, J.-L., Valabregue, R. & Poline, J.-B. Region of Interest Analysis Using an SPM Toolbox. *Neuroimage* **16**, (2002).
71. Hallquist, M. N., Hwang, K. & Luna, B. The nuisance of nuisance regression: spectral misspecification in a common approach to resting-state fMRI preprocessing reintroduces noise and obscures functional connectivity. *NeuroImage* **82**, 208–225 (2013).
72. Lindquist, M. A., Geuter, S., Wager, T. D. & Caffo, B. S. Modular preprocessing pipelines can reintroduce artifacts into fMRI data. *Hum. Brain Mapp.* **40**, 2358–2376 (2019).
73. Mascali, D. *et al.* Evaluation of denoising strategies for task-based functional connectivity: Equalizing residual motion artifacts between rest and cognitively demanding tasks. *Hum. Brain Mapp.* **42**, 1805–1828 (2021).
74. Ciric, R. *et al.* Benchmarking of participant-level confound regression strategies for the control of motion artifact in studies of functional connectivity. *NeuroImage* **154**, 174–187 (2017).
75. Parkes, L., Fulcher, B., Yücel, M. & Fornito, A. An evaluation of the efficacy, reliability, and sensitivity of motion correction strategies for resting-state functional MRI. *NeuroImage* **171**, 415–436 (2018).
76. Chan, M. Y. *et al.* Long-term prognosis and educational determinants of brain network decline in older adult individuals. *Nat. Aging* **1**, 1053–1067 (2021).
77. Wang, J.-H. *et al.* Graph Theoretical Analysis of Functional Brain Networks: Test-Retest Evaluation on Short- and Long-Term Resting-State Functional MRI Data. *PLOS ONE* **6**, e21976 (2011).
78. Fornito, A., Zalesky, A. & Bullmore, E. T. *Fundamentals of brain network analysis*. (Elsevier/Academic Press, 2016).
79. Guimerà, R. & Nunes Amaral, L. A. Functional cartography of complex metabolic networks. *Nature* **433**, 895–900 (2005).
80. Jenkinson, M., Bannister, P., Brady, M. & Smith, S. Improved Optimization for the Robust and Accurate Linear Registration and Motion Correction of Brain Images. *NeuroImage* **17**, 825–841 (2002).
81. R Core Team. *R: A language and environment for statistical computing*. (R Foundation for Statistical Computing, 2021).
82. Bates, D., Mächler, M., Bolker, B. & Walker, S. Fitting linear mixed-effects models using lme4. *J. Stat. Softw.* **67**, 1–48 (2015).
83. Wickham, H. *ggplot2. Elegant Graphics for Data Analysis*. (Springer International Publishing, 2016). doi:10.1007/978-3-319-24277-4.
84. Lüdecke, D. ggeffects: Tidy Data Frames of Marginal Effects from Regression Models. *J. Open Source Softw.* **3**, 772 (2018).

85. Lenth, R. *emmeans: Estimated Marginal Means, aka Least-Squares Means. R package version 1.4.8.* (2020).
86. Gu, Z., Gu, L., Eils, R., Schlesner, M. & Brors, B. circlize Implements and enhances circular visualization in R. *Bioinforma. Oxf. Engl.* **30**, 2811–2812 (2014).
87. Csardi, G. & Nepusz, T. The igraph software package for complex network research. *InterJournal* **Complex Systems**, 1695 (2006).